SF2A 2019
P. Di Matteo, O. Creevey, A. Crida, G. Kordopatis, J. Malzac, J.-B. Marquette, M. N'Diaye, O. Venot (eds)

MODELING THE COMPLEX CHEMISTRY OF HOT CORES IN SAGITTARIUS B2-NORTH: INFLUENCE OF ENVIRONMENTAL FACTORS

M. Bonfand[1], A. Belloche[1], R. T. Garrod[3 2], K. M. Menten[1], E. R. Willis[3], G. Stéphan[3] and H. S. P. Müller[4]

Abstract. Sagittarius B2(N) is host to several hot cores (HCs) in the early stage of star formation, where complex organic molecules (COMs) are detected in the gas phase. Given its exposure to the extreme environment of the Galactic center region, Sgr B2(N) is an excellent target to study the impact of environmental factors on the production of COMs. We combined the analysis of 3mm ALMA data and chemical models to characterize and compare the physical structure and chemical composition of Sgr B2(N)'s HCs. We investigated how the cosmic-ray ionization rate (CRIR) and the minimum dust temperature during the prestellar phase ($T_{\rm min}$) influence the production of COMs. We used COM abundances to constrain the CRIR and $T_{\rm min}$ by comparing the results of chemical models with the observations. Chemical models with $T_{\rm min}$=15 K and a CRIR of 7×10^{-16} s^{-1} best reproduce the abundances observed toward Sgr B2(N)'s HCs.

Keywords: ISM: molecules, astrochemistry, molecular processes, cosmic rays, stars:formation

1 Introduction

The Sagittarius B2 (Sgr B2) molecular cloud is one of the most prominent regions forming high-mass stars in our Galaxy. Located at a projected distance of ∼100 pc from Sgr A*, Sgr B2 is exposed to the extreme environment of the Galactic center (GC) region. A strong interstellar radiation field (1000 G_0, Clark et al. 2013) is expected toward the GC region. Le Petit et al. (2016) derived a cosmic-ray ionization rate (CRIR) in the diffuse gas component of the line of sight to the GC of ζ^{H_2} ∼1–11×10^{-14} s^{-1}, two to three orders or magnitude higher than the standard CRIR (ζ^{H_2} ∼1.3×10^{-17} s^{-1}, Spitzer & Tomasko 1968). Dust continuum measurements carried out with *Herschel* indicate higher temperatures toward the GC region than in the rest of the Galactic disk. Longmore et al. (2012) derived a minimum dust temperature of 19 K toward the GC cloud G0.253+0.016 which shows no strong evidence of star-formation activity. Due to its exceptional characteristics and its proximity to the GC, Sgr B2 provides us with an interesting case study to investigate the influence of environmental factors on the high-mass star formation process and the associated chemistry. In particular, Sgr B2(N), one of the major sites of star formation in Sgr B2, exhibits a rich molecular inventory, including a great variety of complex organic molecules (COMs, see, e.g. Belloche et al. 2017, 2019). For this reason, Sgr B2(N) appears to be an excellent target to improve our understanding of the complex interstellar chemistry.

2 Five hot cores embedded in the same parent cloud

Sgr B2(N) is fragmented into multiple dense and compact objects. On the basis of the 3 mm imaging line survey Exploring Molecular Complexity with ALMA (EMoCA, Belloche et al. 2016), we reported the detection of three new hot cores (HCs), Sgr B2(N3), N4, and N5 (Bonfand et al. 2017, Paper I), in addition to the two already known HCs, Sgr B2(N1) and N2. Ginsburg et al. (2018) later identified 11 star-forming cores at 3 mm within a region of 0.4 pc centered on Sgr B2(N1).

[1] Max-Planck-Institut für Radioastronomie, Auf dem Hügel 69, Bonn, Germany
[2] Departments of Astronomy, University of Virginia, Charlottesville, VA 22904, USA
[3] Departments of Chemistry, University of Virginia, Charlottesville, VA 22904, USA
[4] I. Physikalisches Institut, Universität zu Koöln, Zülpicher Str. 77, 50937 Köln, Germany

© Société Francaise d'Astronomie et d'Astrophysique (SF2A) 2019

By analyzing the EMoCA survey we derived the chemical composition of Sgr B2(N3-N5), identifying 24 distinct species of which about half are complex (Paper I). Figure 1a shows the abundances relative to methanol (CH_3OH) of ten COMs measured toward Sgr B2(N3-N5), as well as Sgr B2(N2) for comparison. The overall chemical composition of Sgr B2(N3) is similar to that of Sgr B2(N5). The abundances of O- and S-bearing species relative to CH_3OH are higher toward Sgr B2(N4) compared to the other HCs, except for NH_2CHO. The chemical composition of Sgr B2(N2) differs significantly from that of Sgr B2(N3-N5). In order to explain the differences in the chemical composition of these four HCs expected to originate from the same cloud material, chemical models are required. In particular we want to derive the CRIR and minimum dust temperature that best characterize the chemical history of Sgr B2(N).

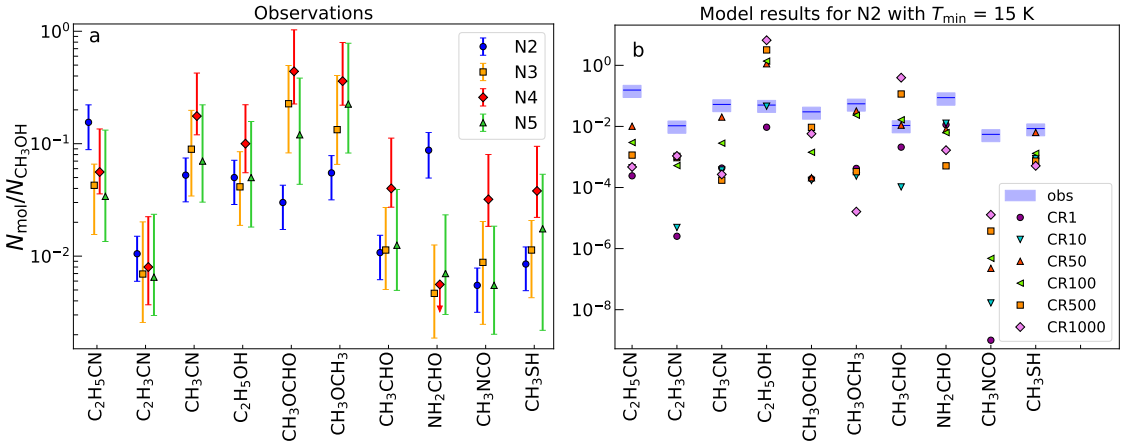

Fig. 1. a: Abundances with respect to CH_3OH of ten COMs detected toward Sgr B2(N2-N5) (Papers I and II). **b:** Abundances with respect to CH_3OH of ten COMs calculated for Sgr B2(N2) by models T15 with different CRIR values. CR1 corresponds to the standard CRIR. The observational values are indicated for comparison with horizontal blue lines and blue boxes represent the 1σ uncertainty.

3 A physical model for high-mass star formation in Sgr B2(N)

Modeling the time-dependent chemical evolution of Sgr B2(N2-N5) requires knowledge of their physical structure and its evolution. We built up a simplified physical model divided into two stages, a prestellar phase followed by the protostellar phase. During the prestellar phase the source undergoes quasi-static contraction at low densities and temperatures. Assuming that all HCs come from the same cloud material, we use the same initial conditions. The protostellar phase starts with the ignition of the central protostar which heats up its free-falling envelope. Our physical model describes the evolution of density and temperature in the envelope of the sources as they evolve from the cold prestellar phase to the present time (Bonfand et al. 2019, Paper II). During the cold, low density phase preceeding the warm up of the envelope, the dust temperature in the outermost layers of the envelope decreases as the density increases. In order to keep the model physically meaningful and to account for the somewhat high dust temperatures expected toward the GC region (see Sect. 1), we defined an arbitrary minimum temperature, $T_{\rm min}$, as the lowest temperature that is allowed in the chemical simulations. Once the central protostar has formed, the temperature in the envelope increases as the protostar's luminosity rises. Based on the estimated time-dependent evolution of the sources' luminosity (Paper II) and the excitation temperatures derived for the HCs at the radius of the COM emission (Paper I), we derived the time-dependent evolution of the dust temperature in the envelope of the sources during the free-fall collapse (Paper II). Given the high densities (Paper I), dust and gas temperatures are assumed to be well coupled during the protostellar phase.

4 Chemical modeling

We used the chemical code MAGICKAL (Model for Astrophysical Gas and Ice Chemical Kinetics and Layering, Garrod 2013) to compute chemical abundances in the envelopes of Sgr B2(N2-N5) (Paper II). We ran for each HC a grid of chemical models varying the minimum dust temperature as follows, $T_{\rm min}$= 10 K (models T10), 15 K (T15) and 20 K (T20); and the CRIR, $\zeta^{\rm H_2}$ from 1.3×10^{-17} s^{-1} (CR1) to 1.3×10^{-14} s^{-1} (CR1000).

4.1 Production of COMs: influence of environmental factors

Figure 2b shows the evolution of the fractional abundances of six COMs during the warm up phase of model T15-CR1 for Sgr B2(N2). The solid-phase abundances of the investigated COMs directly determine their final gas-phase abundances, except for C_2H_3CN. This suggests that the COM gas-phase abundances observed in the warm envelope of Sgr B2(N2) are dominated by the thermal desorption of dust-grain ice mantles. The production of these COMs involves surface reactions between molecules accreted onto dust grains during the earlier, cold prestellar phase, followed by the subsequent sublimation of the dust-grain ice mantles. CH_3OH and C_2H_5OH are already present on the grains with significant abundances before the warm-up phase (*i.e.* at T=15 K, Fig. 2b). This suggests that they mostly form during the earlier cold phase. For instance, CH_3OH form on the grains during the prestellar phase via successive hydrogenation of the CO accreted from the gas phase. The production of CH_3CHO, CH_3OCH_3, and C_2H_3CN is still efficient on the grains up to 30–50 K.

The minimum dust temperature during the prestellar phase has an impact on the production of the main ice constituents (H_2O, CO, CO_2, and CH_3OH), essential to the production of COMs, such that the final gas-phase abundances of the investigated COMs are higher in model T10-CR1 than T15-CR1 (Fig. 2a). The CRIR value has an impact on both the solid- and gas-phase abundances of COMs during the warm-up stage (Fig. 2c). The CRIR influences the dissociation rate of surface species and thus the amount of radicals that can react to form COMs. In the gas phase, the CRIR controls the density of ions and thus the frequency of ion-molecule reactions and electronic recombinations, which both act to form but also destroy COMs.

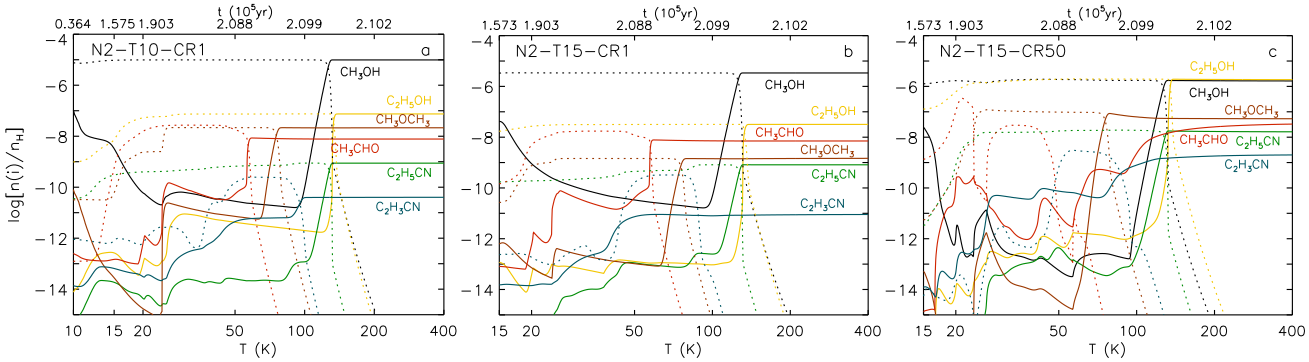

Fig. 2. Fractional abundances (with respect to total hydrogen) of six COMs as a function of the temperature in the envelope of Sgr B2(N2) during the free-fall collapse (Paper II). Results are shown for the chemical models **a:** T10-CR1, **b:** T15-CR1, and **c:** T15-CR50. The solid lines show the fractional abundances in the gas phase while the dotted lines show the abundances on the grains.

4.2 Constraining the environmental factors

Figure 1b compares the gas-phase abundances with respect to CH_3OH observed toward Sgr B2(N2) with the abundance ratios calculated by models T15 with different CRIR values. The [CH_3NCO]/[CH_3OH]] ratio is largely underestimated by all chemical models, suggesting that the binding energy used for CH_3NCO in our chemical models is most likely underestimated (Belloche et al. 2019). For this reason we ignore CH_3NCO in the rest of our analysis. By comparing the observed and calculated abundances it is possible to constrain $T_{\rm min}$ and $\zeta^{\rm H_2}$ that best characterize Sgr B2(N)'s HCs. Given the uncertainties on the observed abundances and the results of chemical models, we consider the agreement between model and observations to be reasonable when the calculated abundances are within one order of magnitude from the observed values. Figure 3a shows the matrix of confidence levels computed for nine COMs relative to CH_3OH, for Sgr B2(N2-N5) taken together. A confidence level of 32% indicates that the calculated abundances lie one order of magnitude lower/higher than the observed ones (Paper II). Given that all HCs should be exposed to the same cosmic-ray flux and probably shared a similar thermal history during the prestellar phase, our analysis shows that, with a confidence level of 37.5%, models T15-CR50 (*i.e.* $\zeta^{\rm H_2} = 6.5{\times}10^{-16}$ s^{-1} and $T_{\rm min}$ = 15 K) best match the observations. In Fig. 3b we examine in more detail how the abundance ratio of two chemically linked species, the cyanides C_2H_3CN and C_2H_5CN, is affected by the CRIR. [C_2H_5CN]/[C_2H_3CN] decreases by several orders of magnitude as the CRIR increases. The observed ratio is best reproduced by model CR50, which is consistent with the result derived overall for the nine COMs from the matrix of confidence level.

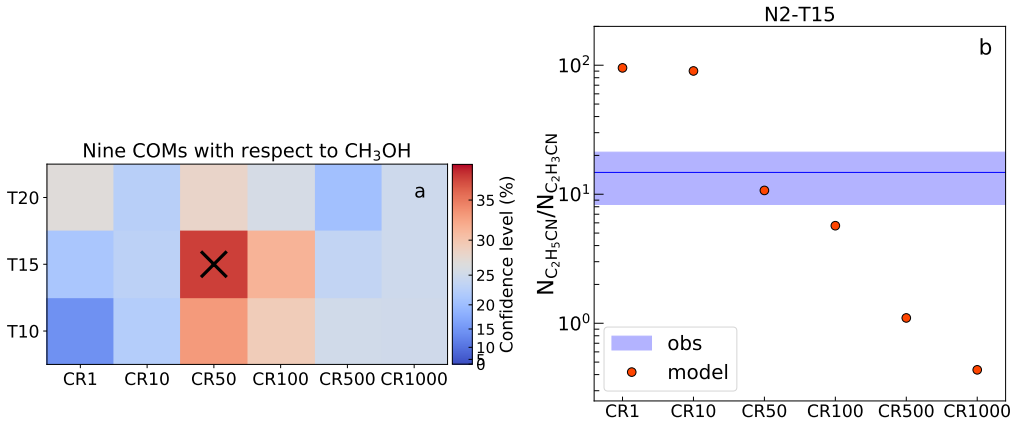

Fig. 3. a: Matrix of confidence level of the chemical models with the observations, for Sgr B2(N2-N5) taken together, and for the abundances of nine COMs with respect to CH_3OH (Paper II). The black cross shows the best-fit model. **b:** Abundances of C_2H_5CN with respect to C_2H_3CN as a function of the CRIR for model N2-T15 (Paper II). The horizontal blue line shows the ratio observed toward Sgr B2(N2) with the blue box that represents the 1σ uncertainty.

5 Conclusion

We combined the analysis of the 3 mm imaging line survey EMoCA and the chemical modeling of Sgr B2(N)'s HCs to present the first detailed comparative study of four HCs evolving in the same environment. We investigated the influence of cosmic-ray ionization and minimum dust temperature during the prestellar phase on the production of selected COMs. In the chemical simulations all investigated COMs mainly form on the surface of dust grains, followed by later desorption into the gas phase. While the production of CH_3OH and C_2H_5OH mostly relies on the cold prestellar phase, CH_3CHO, CH_3OCH_3, and C_2H_3CN still form efficiently on the grains up to 30–50 K. We used COMs as indirect probes to constrain Sgr B2(N)'s environmental conditions by comparing the observations with the results of chemical models. It showed that a minimum temperature of 15 K, higher than the low values used in previous studies ($\leq$10 K, see, e.g., Belloche et al. 2017; Garrod et al. 2017) and closer to the lowest temperature measured toward the GC region (19 K, Sect. 1), leads to an efficient production of COMs roughly consistent with the abundances measured in Sgr B2(N)'s HCs. For models with $T_{\rm min}$ = 20 K signs of disagreement emerge between models and observations, but it could be that models with $T_{\rm min}$ =17–18 K produce COMs in amounts that are still consistent with the observations. Furthermore, the coldest dust grains in the GC region may be masked by warmer outer layers and thus have been missed by *Herschel* because of its limited angular resolution. Therefore, it is likely that the constraint we derived on $T_{\rm min}$ from the COM abundances is consistent with the thermal properties of the GC region. Finally, the best match between chemical models and observations is obtained for $\zeta^{\rm H_2} = 6.5{\times}10^{-16}$ s^{-1}, which is a factor 50 higher than the standard CRIR. This is somewhat lower than extreme values expected toward the diffuse medium in the GC region (see Sect. 1). This difference may reflect the attenuation of cosmic rays in denser gas.

References

Belloche, A., Garrod, R. T., Müller, H. S. P., et al. 2019, Astronomy and Astrophysics, 628, A10
Belloche, A., Meshcheryakov, A. A., Garrod, R. T., et al. 2017, A&A, 601, A49
Belloche, A., Müller, H. S. P., Garrod, R. T., & Menten, K. M. 2016, A&A, 587, A91
Bonfand, M., Belloche, A., Garrod, R. T., et al. 2019, Astronomy and Astrophysics, 628, A27
Bonfand, M., Belloche, A., Menten, K. M., Garrod, R. T., & Müller, H. S. P. 2017, A&A, 604, A60
Clark, P. C., Glover, S. C. O., Ragan, S. E., Shetty, R., & Klessen, R. S. 2013, ApJ, 768, L34
Garrod, R. T. 2013, ApJ, 765, 60
Garrod, R. T., Belloche, A., Müller, H. S. P., & Menten, K. M. 2017, A&A, 601, A48
Ginsburg, A., Bally, J., Barnes, A., et al. 2018, ApJ, 853, 171
Le Petit, F., Ruaud, M., Bron, E., et al. 2016, A&A, 585, A105
Longmore, S. N., Rathborne, J., Bastian, N., et al. 2012, ApJ, 746, 117
Spitzer, J. L. & Tomasko, M. G. 1968, ApJ, 152, 971